The Rab GTPase activating protein TBC-2 extends longevity by facilitating release of FOXO/DAF-16 from endosomes

İçten Meraş[1,2,3], Laëtitia Chotard[2,4], Thomas Liontis[3,5,6], Zakaria Ratemi[3], Benjamin Wiles[3], Jung Hwa Seo[3], Jeremy M. Van Raamsdonk[3,4,5,6] and Christian E. Rocheleau[1,2,3,4]*

[1]Department of Anatomy and Cell Biology, McGill University, Montreal, Canada; [2]Division of Endocrinology and Metabolism, Department of Medicine, McGill University, Montreal, Canada; [3] Metabolic Disorders and Complications Program, Centre for Translational Biology, Research Institute of the McGill University Health Centre, Montreal, Canada; [4]Division of Experimental Medicine, Department of Medicine, McGill University, Montreal, Canada; [5]Department of Neurology and Neurosurgery, McGill University, Montreal, Canada; [6]Brain Repair and Integrative Neuroscience Program, Centre for Translational Biology, Research Institute of the McGill University Health Centre, Montreal, Canada

*Correspondence: Christian E. Rocheleau (christian.rocheleau@mcgill.ca)

Running title: Endosomal Regulation of FOXO transcription factors

ABSTRACT

FOXO transcription factors have been shown to regulate longevity in model organisms and are associated with longevity in humans. To gain insight into how FOXO functions to increase lifespan, we examined the subcellular localization of DAF-16 in *C. elegans.* We show that DAF-16 is localized to endosomes and that this endosomal localization is increased by the insulin-IGF signaling (IIS) pathway. Endosomal localization of DAF-16 is also increased by disrupting the Rab GTPase activating protein TBC-2, or decreased by inhibiting the RAB-5 or RAB-7 GTPases, key regulators of early to late endosome maturation. Importantly, the amount of DAF-16 that is localized to endosomes has functional consequences as increasing endosomal localization through mutations in *tbc-2* decreased the lifespan of long-lived *daf-2 IGFR* mutants, depleted their fat stores, and DAF-16 target gene expression. Finally, we show that the ability of TBC-2 proteins, TBC1D2 and TBC1D2B, to regulate FOXO protein localization is conserved in human cells. Overall, this work identifies endosomal localization as a mechanism regulating FOXO/DAF-16, which is important for its functions in metabolism and aging.

35 **INTRODUCTION**

36

37 Insulin/insulin-like growth factor signaling (IIS) is an evolutionarily conserved pathway
38 that plays an important role in lifespan, development, metabolism, immunity and stress responses
39 from *Caenorhabditis elegans* to humans (Accili and Arden, 2004; Barthel *et al.*, 2005; Greer and
40 Brunet, 2005; Murphy and Hu, 2013). IIS-mediated regulation of *C. elegans* FOXO, DAF-16,
41 were first identified via genetic characterization of mutants affecting dauer (an alternative stress
42 resistant larval stage) and life span (Riddle *et al.*, 1981; Kenyon *et al.*, 1993; Lin *et al.*, 1997;
43 Ogg *et al.*, 1997). For example, animals that have a mutation in their insulin-like growth factor
44 receptor (IGFR), DAF-2, live almost two times longer than wild type animals in a DAF-16-
45 dependent manner (Kenyon *et al.*, 1993). Under favorable conditions, the *C. elegans* DAF-2
46 IGFR signals through a conserved PI3K/Akt pathway to phosphorylate and inhibit nuclear
47 accumulation of DAF-16 FOXO (Murphy and Hu, 2013). In short, DAF-2 IGFR activation
48 leads to the activation of AGE-1 PI3K which phosphorylates PI(4,5)P_2 to generate PI(3,4,5)P_3
49 which can bind and recruit PDK-1 and AKT-1/2 kinases. DAF-18 PTEN, a lipid and protein
50 phosphatase, countacts AGE-1 PI3K and thus negatively regulates signaling. PDK-1 activates
51 AKT-1/2 which in turn phosphorylates DAF-16 creating binding sites for PAR-5 and FTT-2 14-
52 3-3 scaffold proteins that sequester DAF-16 FOXO in the cytoplasm. During adverse conditions
53 such as starvation, IIS is suppressed and DAF-16 FOXO enters the nucleus to induce the
54 expression of stress response genes. As such, DAF-16 FOXO mediates most *daf-2 IGFR* mutant
55 phenotypes.

56 Upon activation, the Insulin/IGF receptor is internalized into endosomes, where it can
57 disassociate from its ligand and recycle back to the plasma membrane, or it can be targeted for
58 lysosomal degradation (Bergeron *et al.*, 2016). The identification of activated IGFR on
59 endosomes suggested that endosomes can serve as a platform for signaling (Baass *et al.*, 1995).
60 Subsequently, several components of the IIS pathway have been shown to localize on
61 endosomes. PTEN localizes on PI3P positive endosomes through its C2 domain and has been
62 demonstrated to regulate endosome trafficking via dephosphorylation of Rab7 (Naguib *et al.*,
63 2015; Shinde and Maddika, 2016). Akt2 localizes to Appl-1 and WDFY-2 positive endosomes to
64 get fully activated and regulate AKT2 specific downstream substrates (Schenck *et al.*, 2008;
65 Walz *et al.*, 2010). 14-3-3 proteins can interact with several AKT phosphorylation targets to
66 regulate their subcellular localization and have been found on endosomes (Jungmichel *et al.*,
67 2014; Marat *et al.*, 2017). However, a role for endosome trafficking in regulation of FOXO
68 transcription factors has not been demonstrated to the best of our knowledge.
69 Rab5 and Rab7 GTPases localize to early and late endosomes respectively and are critical
70 regulators of trafficking to the lysosome, an organelle important for cargo degradation and
71 metabolic signaling (Huotari and Helenius, 2011; Settembre *et al.*, 2013). Like many small
72 GTPases, Rabs cycle between a GTP-bound active state and GDP-bound inactive state. This
73 cycling requires guanine nucleotide exchange factors for activation and GTPase Activating
74 proteins (GAPs) to catalyze GTP hydrolysis and hence Rab inactivation. We previously
75 characterized *C. elegans* TBC-2 as having *in vitro* GAP activity towards RAB-5, and some
76 activity towards RAB-7 (Chotard *et al.*, 2010a). Mutations in *tbc-2* result in enlarged late
77 endosomes in several tissues including the intestine, an important site of IIS and metabolic

78 regulation (Libina *et al.*, 2003). In addition to early to late endosome maturation, TBC-2
79 regulates phagosome maturation (Li *et al.*, 2009), dense core vesicle maturation (Sasidharan *et*
80 *al.*, 2012) endosome recycling as an effector of RAB-10 and CED-10/Rac (Sun *et al.*, 2012; Liu
81 and Grant, 2015) and yolk protein trafficking in oocytes and embryos (Chotard *et al.*, 2010b).
82 Yolk protein is prematurely degraded in *tbc-2* mutants. As such, *tbc-2* mutant larvae hatched in
83 the absence of food had reduced survival during L1 (first larval stage) diapause (Chotard *et al.*,
84 2010b). TBC-2 has two human homologs TBC1D2/Armus and TBC1D2B (Chotard *et al.*,
85 2010a). TBC1D2 has *in vitro* GAP activity toward Rab7 and regulates endosome trafficking and
86 autophagy (Frasa *et al.*, 2010; Serva *et al.*, 2012; Carroll *et al.*, 2013; Toyofuku *et al.*, 2015;
87 Jaber *et al.*, 2016). TBC1D2B interacts with Rab22 and Rab31, Rab5 related GTPases, and
88 colocalizes with Rab5 and Rab7, but a specific Rab GTPase target of GAP activity has not been
89 demonstrated (Kanno *et al.*, 2010; Manshouri *et al.*, 2019; Harms *et al.*, 2020; Wei *et al.*, 2021).
90 Here we explore the subcellular localization of DAF-16 and show that DAF-16 localizes
91 to endosomes in *C. elegans* intestinal cells. We found that endosome localization is regulated by
92 nutrient availability and IIS. We show that endosome localization is increased through mutations
93 in *tbc-2*, at the expense of nuclear localization. The increased endosomal localization of DAF-16
94 decreases lifespan, fat storage and DAF-16 target gene expression in *daf-2 IGFR* mutant animals.
95 In human cell lines we demonstrated that phosphorylated FOXO1/3a localizes to endosomes and
96 that this localization is regulated by TBC1D2/Armus and TBC1D2B. Combined these results
97 demonstrate a role of endosomal localization in the regulation and function of FOXO, which is
98 conserved between *C. elegans* and humans.
99
100

101 **RESULTS**
102

103 **TBC-2 regulates DAF-16 localization to endosomes in the intestine**

104 We previously reported that *tbc-2* is required for survival during L1 diapause (Chotard *et*
105 *al.*, 2010b). Since *daf-16* is also required for survival during L1 diapause (Munoz and Riddle,
106 2003; Baugh and Sternberg, 2006) we sought to test whether TBC-2 might regulate the nuclear
107 versus cytoplasmic localization of DAF-16. Although we determined that loss of *tbc-2* did not
108 result in precocious development during L1 diapause as seen *daf-16* mutants (Baugh and
109 Sternberg, 2006; Chotard *et al.*, 2010b), we found that TBC-2 does in fact regulate DAF-16
110 localization. Unexpectedly, we found that DAF-16a::GFP (*zIs356*) localized to numerous
111 amorphous vesicles in the intestinal cells of *tbc-2(tm2241)* deletion mutant animals (Figure 1B).
112 Furthermore, we found that DAF-16a::GFP localized to vesicles in the intestine of wild-type
113 animals (Figure 1A). The percentage of hermaphrodites with DAF-16 vesicles increased during
114 larval development, peaking at L4 and young adults (Figure 1I; Figure S1A). *tbc-2(tm2241)*
115 animals were about twice as likely to have DAF-16 vesicles than wild-type (Figure 1J; Figure
116 S1A). We quantified the number of vesicles per animal. Wild-type animals can range from zero
117 vesicles to having hundreds of vesicles (Figure 1I). Vesicles can be distributed throughout the
118 20 cells of the intestine, or can be present in high numbers in just one or a few intestinal cells. In
119 contrast, *tbc-2(tm2241)* animals typically have many more vesicles than wild-type (Figure 1J;
120 Figure S1A). Although DAF-16a::GFP nuclear localization is low in normal growth conditions,
121 we find that *tbc-2(tm2241)* intestinal nuclei appear to have less nuclear DAF-16a::GFP than
122 wild-type (Figure 1A and B). We quantified the fluorescence intensity of DAF-16a::GFP in
123 nuclei of *tbc-2(tm2241)* intestinal cells comparing nuclei of cells with vesicles versus nuclei of

124 cells without vesicles (Figure 1K). We found that nuclei of cells with vesicles have significantly
125 less nuclear DAF-16a::GFP than cells without vesicles. Thus, DAF-16 localizes to vesicles in
126 wild-type and *tbc-2(tm2241)* animals, and *tbc-2(tm2241)* animals have less nuclear DAF-
127 16a::GFP, likely due to sequestration to cytoplasmic vesicles.

128 To determine if endogenous DAF-16 localizes to vesicles we analyzed *daf-16(hq23)*, a
129 DAF-16::GFP line generated by CRISPR/Cas9 genome editing and generously provided by M.-
130 Q. Dong, and found that endogeneously tagged DAF-16 localized to vesicles in both wild-type
131 and *tbc-2(tm2241)* mutants (Figure S2A-F). We also analyzed three other transgenic strains with
132 lower expression levels than DAF-16a::GFP (*zIs356*): GFP::DAF-16a (*muIs71*), DAF-16a::RFP
133 (*lpIs12*) and DAF-16f::GFP (*lpIs14,* with an alternate N-terminus)(Henderson and Johnson,
134 2001; Lin *et al.*, 2001; Kwon *et al.*, 2010). While we were unable to detect DAF-16 positive
135 vesicles in wild-type backgrounds, in *tbc-2(tm2241)* mutant animals there were DAF-16 vesicles
136 in all three transgenic animals (Figure S2G-X). To determine if vesicular localization is specific
137 to DAF-16::GFP, we overexpressed GFP by itself in the intestine. Overexpression of GFP from
138 *vha-6* intestinal specific promoter, *vhEx1[Pvha-6::GFP]*, did not show significant vesicular
139 localization in wild-type animals (Figure S1B). In *tbc-2(tm2241)* animals GFP showed some
140 vesicular localization and potential aggregates, but much less than seen with DAF-16a::GFP,
141 indicating that the vesicular localization is due to DAF-16 and not the fluorescent tag. Of note,
142 we found that GFP expression in the *tbc-2* background was visibly stronger than in wild-type
143 (Figure S1C-F), consistent with *vha-6* ranking amongst the top downregulated DAF-16-
144 responsive genes (Tepper *et al.*, 2013) and consistent with TBC-2 facilitating DAF-16 nuclear
145 localization.

146 The finding that DAF-16 localizes to enlarged vesicles in *tbc-2* mutants and that DAF-16
147 vesicles contain autofluorescent lipofuscin (Figure 1E-H), a hallmark of intestinal
148 endolysosomes (Clokey and Jacobson, 1986), suggested that DAF-16 vesicles are endosomal.
149 To determine if the DAF-16 vesicles are endosomes, we co-expressed DAF-16a::GFP with
150 RFP::RAB-5, an early endosomal marker, or with mCherry::RAB-7, a late endosomal marker
151 (Chavrier *et al.*, 1990; Sato *et al.*, 2005; Chen *et al.*, 2006). We found that in wild-type animals,
152 DAF-16a::GFP localizes to a subset of RAB-5 and RAB-7-positive endosomes (Figure 2A-F).
153 Furthermore, we tested the genetic requirements for *rab-5* and *rab-7* for DAF-16 localization by
154 RNAi. We found that *rab-5(RNAi)* and *rab-7(RNAi)* knockdown significantly decreased the
155 number of wild-type and *tbc-2(tm2241)* animals with DAF-16a::GFP vesicles (Figure 2G and
156 H). Together, these data are consistent with DAF-16 localizing to a sub-population of endosomes
157 or endosome-like vesicles in the intestinal cells.
158
159 **Acute starvation suppresses DAF-16 localization to endosomes**
160 Nuclear localization of DAF-16 is modulated by nutrient availability. As such, starvation
161 promotes DAF-16 cytoplasmic-to-nuclear shuttling (Henderson and Johnson, 2001). Therefore,
162 we tested the effect of acute starvation on DAF-16a::GFP localization to endosomes. We found
163 that starvation strongly suppressed the localization of DAF-16 to endosomes in both wild-type
164 and *tbc-2(tm2241)* mutants (Figure 3A; Figure S3). Upon re-feeding, DAF-16 relocalized to
165 endosomes after 1-2 hours, in both wild-type and *tbc-2(tm2241)* mutants. Thus, DAF-16
166 localization on endosomal membranes is regulated by nutrient availability.
167

168 **Insulin/IGF signaling regulates DAF-16 localization to endosomes**

169 To determine if IIS regulates DAF-16 localization to endosomes we analyzed the effect
170 of disrupting IIS on DAF-16a::GFP localization (see Figure 3B for reference). Firstly, we
171 analyzed a hypomorphic mutant of the insulin/IGF receptor, *daf-2(e1370)*, in which IIS is
172 reduced, particularly at higher temperatures (Swanson and Riddle, 1981). We compared DAF-
173 16a::GFP localization in three independent *daf-2(e1370)* strains at 15°C and shifted overnight to
174 25°C. All three showed a significant reduction in the number of DAF-16 positive vesicles at
175 25°C, while the wild-type strain did not (Figure 3C), indicating that DAF-2 promotes DAF-16
176 localization to endosomes.

177 DAF-18, the homolog of human tumor suppressor protein PTEN, acts as a negative
178 regulator of the IIS pathway counteracting AGE-1 PI3K signaling by dephosphorylating
179 3'phosphate on the PI(3,4,5)P_3 converting it to PI(4,5)P_2 (Ogg and Ruvkun, 1998). We analyzed
180 DAF-16a::GFP localization in the *daf-18* reference allele, *e1375.* We generated three
181 independent *daf-18(e1375); zIs356* strains, but only two strains had increased endosome
182 localization of DAF-16, but cumulatively the three strains had a statistically significant increase
183 in the number of animals with DAF-16 endosomes (Figure 3D). Since *daf-18(e1375)* is possibly
184 a non-null allele, we analyzed a deletion allele, *daf-18(ok480).* We found that five independent
185 *daf-18(ok480); zIs356* strains had more DAF-16 endosomes than wild-type that cumulatively
186 was statistically significant (Figure 3D). Since DAF-16 endosome localization is increased in
187 the background of two distinct *daf-18* alleles, it is consistent with increased IIS causing an
188 increase in DAF-16 localization to endosomes.

189 *C. elegans* AKT-1 and AKT-2 function upstream of, and can phosphorylate, DAF-16
190 (Paradis and Ruvkun, 1998; Hertweck *et al.*, 2004). We found that animals with an *akt-2(ok393)*
191 deletion mutation, there was an insignificant decrease in DAF-16 endosomal localization in two
192 independent strains (Figure 3E). However, in *akt-1*(*RNAi)* animals, we observed a significant
193 decrease in DAF-16 endosomal localization where DAF-16 localized mainly to the nucleus,
194 compared to the control animals in three independent experiments (Figure 3F). Therefore, AKT-
195 1 is the main kinase regulating DAF-16 localization to endosomes.
196 Phosphorylation of FOXO proteins by Akt creates binding sites for 14-3-3 proteins,
197 which promote cytoplasmic retention of FOXO (Brunet *et al.*, 1999). *C. elegans* has two genes
198 that encode for 14-3-3 proteins that interact with DAF-16, *par-5* and *ftt-2* (Wang and Shakes,
199 1997; Morton *et al.*, 2002; Wang *et al.*, 2006). We found that *ftt-2(RNAi)*, but not *par-5(RNAi)*,
200 suppressed the localization of DAF-16 to endosomes (Figure 3G), suggesting that FTT-2
201 regulates DAF-16 endosomal localization.
202 To determine if AKT phosphorylation regulates DAF-16 localization to endosomes we
203 tested if DAF-16a^{AM}::GFP *muIs113*, in which the four consensus AKT phosphorylation sites
204 (T54A, S240A, T242 and S314A) are mutated to alanine (Lin *et al.*, 2001), could still localize to
205 vesicles in *tbc-2(tm2241)* mutants. Since the expression levels are lower than DAF-16a::GFP
206 *zIs356*, we used GFP::DAF-16a *muIs71* with comparable expression levels as control. We found
207 that the number of *tbc-2(tm2241)* animals with DAF-16a^{AM}::GFP positive vesicles was
208 significantly less than the GFP::DAF-16a control (Figure 3H). Together, these data demonstrate
209 that IIS regulates endosomal DAF-16 through AKT-1 specific phosphorylation and FTT-2 14-3-
210 3.

211

212 **TBC-2 is required for lifespan extension and increased fat storage of *daf-2(e1370)* mutants**

213 To determine if the increased endosomal localization of DAF-16 seen in *tbc-2* mutants
214 affects DAF-16 activity, we tested if TBC-2 regulates adult lifespan. We found that the *tbc-*
215 *2(sv41)* and *tbc-2(tm2241)* deletion alleles had similar lifespans as compared to wild-type
216 (Figure 4A and B). As expected, *daf-2(e1370)* animals lived significantly longer than wild-type.
217 We found that both *tbc-2* alleles significantly shortened the lifespan of *daf-2(e1370)* animals
218 (Figure 4A and B). Thus, TBC-2 is not required for normal lifespan, but is partly required for
219 the extended lifespan of *daf-2(e1370)* mutants.

220 To assess TBC-2's contribution to other *daf-2* mutant phenotypes, we tested whether
221 TBC-2 is required for the increased fat storage of *daf-2(e1370)* mutants. Consistent with
222 previous findings we found that *daf-2(e1370)* had significantly more fat than wild-type animals
223 as determined by Nile Red and Oil Red O staining of fixed L4 larvae (Kimura *et al.*, 1997;
224 O'Rourke *et al.*, 2009) (Figure 4C-F). We found that *tbc-2(tm2241)* larvae had less fat than wild-
225 type with Nile Red staining, but not with Oil Red O staining (Figure 4D and F). This difference
226 might reflect the lower sensitivity of Oil Red O for quantifying lipid abundance as compared to
227 Nile Red (Escorcia *et al.*, 2018). Interestingly, we found that *tbc-2(tm2241)* significantly
228 suppressed the *daf-2(e1370)* increased lipid staining by both Nile Red and Oil Red O (Figure 4C-
229 F). Thus, TBC-2 is required for the increased fat storage of *daf-2(e1370)* mutants.

230 The fact that TBC-2 is required for the increased longevity and increased fat storage of
231 *daf-2(e1370)* mutants suggests that TBC-2 could be a negative regulator of IIS. Therefore, we
232 tested if *tbc-2* mutants regulate DAF-16 target gene expression in *daf-2(e1370)* animals. We

233 used qRT-PCR to measure the expression of DAF-16 target genes in wild-type, *daf-2(e1370),*
234 *tbc-2* mutants and *tbc-2; daf-2* double mutants. Consistent with previous reports, the expression
235 of six of the DAF-16 target genes were upregulated in *daf-2(e1370)* animals (Figure 5) (Honda
236 and Honda, 1999; Murphy *et al.*, 2003; Ackerman and Gems, 2012; Tepper *et al.*, 2013). While
237 *tbc-2(tm2241)* and *tbc-2(sv41)* did not appreciably alter DAF-16 target gene expression relative
238 to wild-type, both reduced the expression of *sod-3, dod-3, gpd-2* and *icl-1* in *daf-2(e1370)*
239 mutants, while *mtl-1* and *ftn-1* were not significantly decreased (Figure 5). The fact that TBC-2
240 was required for the increased expression of four of six DAF-16 target genes with elevated
241 expression in *daf-2(e1370)* mutants suggests a more specific role for TBC-2 in regulating DAF-2
242 to DAF-16 signaling.
243
244 **TBC1D2 and TBC1D2B regulate phospho-FOXO1/3a localization to endosomes**
245 Towards understanding if endosomal regulation of FOXO proteins occurs in human cells,
246 we tested if FOXO proteins localize to endosomes and if this localization is regulated by the
247 human homologs of TBC-2, TBC1D2 and TBC1D2B. We confirmed that TBC1D2 and
248 TBC1D2B were expressed in Henrietta Lacks (HeLa) and Human Embryonic Kidney 293
249 (HEK293) cells. TBC1D2 mRNA and protein were more highly expressed in HeLa cells while
250 TBC1D2B mRNA and protein are more highly expressed in HEK293 cells (Figure S4). siRNAs
251 targeting TBC1D2 and TBC1D2B specifically and strongly reduced the expression in both cell
252 lines (Figure S5). We assessed the levels of total FOXO1 and FOXO3a as well as the relative
253 levels of phosphorylated FOXO1 (pFOXO1) and pFOXO3a in HeLa and HEK293 cells treated
254 with siRNA targeting TBC1D2, TBC1D2B or both (Figure S6). We did not detect a significant

255 difference in the levels of total FOXO1 or FOXO3a relative to Actin, indicating that TBC1D2
256 and TBC1D2B do not regulate FOXO1/3a protein levels. Furthermore, the ratio of pFOXO1 and
257 pFOXO3a relative to total FOXO1 and FOXO3a respectively is not significantly different
258 suggesting that the phosphorylation status of FOXO1 and FOXO3a is not regulated by TBC1D2
259 and TBC1D2B. We assayed the colocalization of FOXO3a, the predominant FOXO in HEK293
260 and HeLa cells and closest DAF-16 homolog, with endogenous Rab5 and Rab7 early and late
261 endosomal GTPases. FOXO3a is primarily found in the nucleus of HeLa cells and is both
262 cytoplasmic and nuclear in HEK293 cells, as such there is a higher correlation coefficient of
263 FOXO3a with Rab5 and Rab7 in untreated HEK293 cells than in HeLa cells (Figure S7). Thus,
264 FOXO3a localizes to endosomes in human cells. Knockdown of TBC1D2 and TBC1D2B by
265 siRNA had no effect on FOXO3a colocalization with Rab5 and Rab7 in HEK293 cells (Figure
266 S7 A-D). In HeLa cells there was a modest, but significant increase in colocalization of
267 FOXO3a with Rab5 and Rab7, but with only one set of siRNAs targeting both TBC1D2 and
268 TBC1D2B (Figure S7 E-H).

269 Since our data with DAF-16 suggests that endosome localization correlates with
270 phosphorylated DAF-16, we analyzed the localization of pFOXO1/3a using an antibody that
271 recognizes both phosphorylated FOXO1 and FOXO3a. In HEK293 cells there was a clear
272 increase in colocalization of phosphorylated FOXO1/3a with Rab5 and a moderate increase with
273 Rab7 when both TBC1D2 and TBC1D2B were knocked down with two distinct siRNAs (Figure
274 6 A-D). This was even more evident in HeLa cells where individual knockdown of TBC1D2 or
275 TBC1D2B was sufficient to significantly increase colocalization of pFOXO1/3a with Rab5 and
276 knockdown of both TBC1D2 and TBC1D2B strongly increased colocalization with both Rab5

277 and Rab7 (Figure 6 E-H). These results show that FOXO proteins localize to endosomes in
278 human cells and that similar to the *C. elegans* intestinal cells, this localization is regulated by the
279 TBC1D2 family of RabGAPs.

280 The modest colocalization seen in HeLa cells appeared to coincide with increased
281 cytoplasmic FOXO3a in TBC1D2 and TBC1D2B knockdown cells (Figure S7). Therefore, we
282 measured the nuclear fluorescence intensity of pFOXO1/3a and total FOXO3a relative to DAPI
283 and found that siRNA knockdown of TBC1D2 and TBC1D2B together or individually both
284 reduced the nuclear localization of FOXO3a in HeLa cells (Figure 7F, H). As expected the
285 correlation of coefficient of pFOXO1/3a with DAPI was low in comparison to FOXO3a and not
286 altered by knockdown of TBC1D2 and TBC1D2B (Figure 7E, G). In HEK293 cells, knockdown
287 of TBC1D2B but not TBC1D2 was sufficient to reduce nuclear localization of both total
288 FOXO3a and pFOXO1/3a (Figure 7A-D), consistent with TBC1D2B being more highly
289 expressed in HEK293 cells than TBC1D2. These data indicate that the increased endosomal
290 localization of FOXO protein correlates with decreased nuclear localization mirroring our data
291 with DAF-16 in *C. elegans* intestinal cells and that there is a conserved role for TBC-2/TBC1D2
292 family of RabGAPs in regulation of FOXO proteins.
293
294
295
296

297 **DISCUSSION**

298 Endosome trafficking and signal transduction are intimately linked processes regulating signal
299 propagation, specificity and attenuation (Miaczynska, 2013; Bergeron *et al.*, 2016). However,
300 there remains a large knowledge gap in the spatial regulation of cell signaling and where
301 downstream transcription factors are regulated. We identified a previously unknown localization
302 for FOXO transcription factors on endosomes in *C. elegans* and in human cell lines. Endosome
303 localization is limited by the TBC1D2 family of Rab GAPs. Loss of *C. elegans* TBC-2 or
304 knockdown of human TBC1D2 and TBC1D2B results in increased endosomal localization of
305 FOXO proteins at the expense of nuclear localization. As such, *C. elegans* TBC-2 is partly
306 required for several *daf-2 IGFR* mutant phenotypes including lifespan extension, increased fat
307 storage, and increased DAF-16 target gene expression that result from DAF-16 nuclear
308 translocation. DAF-16 endosome localization is largely dependent on IIS consistent with this
309 being a phosphorylated, inactive pool of DAF-16. Together our data show that the TBC1D2
310 family of Rab GAPs have an evolutionarily conserved role in regulating the balance of nuclear
311 versus endosomal localization of FOXO transcription factors.

312

313 **DAF-16 localizes to endosomes**

314 We were surprised to find that DAF-16 FOXO localizes to a subset of RAB-5 and RAB-7
315 endosomes in wild-type animals. Many studies have used DAF-16 cytoplasmic versus nuclear
316 localization to assess IIS activity under various conditions. We assume that DAF-16 positive
317 endosomes were not discovered earlier as nuclear translocation can be assessed at low
318 magnification, and DAF-16 positive endosomes are not present in every cell or every animal.

319 Furthermore, we first took notice of DAF-16 positive endosomes in the *tbc-2* mutant background
320 where they are more prominent. These are likely not an artefactual consequence of
321 overexpression, as we see these vesicles in the endogenously tagged *daf-16::GFP* and we do not
322 see similar vesicles in a GFP overexpression strain. Additionally, DAF-16-vesicles are regulated
323 by IIS and we detect endogenous FOXO on endosomes in human cells (discussed further below).
324 Many components of the IIS pathway localize to endosomes in mammalian cells
325 including active insulin receptor and downstream signaling components such as PI3K, Akt,
326 PTEN and 14-3-3 proteins (Khan *et al.*, 1986; Christoforidis *et al.*, 1999; Balbis *et al.*, 2000;
327 Braccini *et al.*, 2015; Naguib *et al.*, 2015; Bergeron *et al.*, 2016; Marat *et al.*, 2017; Kim *et al.*,
328 2018). In the case of Akt and PTEN, both have demonstrated roles in regulation of endosome
329 trafficking independent of IIS (Shinde and Maddika, 2016, 2017; Mondin *et al.*, 2019; Hsu *et al.*,
330 2020). On the other hand, the PI3Ks are Rab5 effectors and Rab5 has been shown to promote
331 Akt activity on endosomes (Christoforidis *et al.*, 1999; Shin *et al.*, 2005; Su *et al.*, 2006; Cheng
332 *et al.*, 2009; Braccini *et al.*, 2015). While endosomal localization of FOXO proteins has not been
333 reported to the best of our knowledge, knockdown of Rab5 in mouse liver results in a strong
334 increase in phosphorylated FOXO1 (Zeigerer *et al.*, 2015). This is contrary to the finding that
335 Rab5 promotes Akt phosphorylation (Su *et al.*, 2006; Braccini *et al.*, 2015), which could be a
336 consequence of indirect regulation or suggest tissue-specific regulation. The fact that TBC-2 is a
337 RAB-5 GAP is consistent with increased RAB-5 activity promoting DAF-16 localization on
338 endosomes. This is further supported by the fact that *rab-5* and *rab-7* RNAi knockdown reduces
339 the number of animals with DAF-16 vesicles in both wild-type and *tbc*-2 mutants. Given the

340 importance of RAB-5 for endosome trafficking, it is difficult to parse whether RAB-5 is
341 promoting a platform for DAF-16 localization or if it also has a role in IIS.
342 We demonstrated that DAF-16 localized to a subset of RAB-5 and RAB-7 positive
343 endosomes. Since RAB-5 and RAB-7 promote trafficking to the lysosome and promote receptor
344 tyrosine kinase degradation, it is possible that DAF-16-positive endosomes are signaling
345 endosomes, in which case we would expect other upstream signaling components might be
346 present. Consistent with that hypothesis, knockdown of IIS reduces the number of animals with
347 DAF-16 vesicles. However, when analyzing DAF-16 localization in *daf-2(e1370)* mutants at
348 15°C vs. 25°C, we find that while there is a reduction in the number of DAF-16 endosomes,
349 these endosomes are noticeably fainter at 25°C. This suggests that there are not necessarily less
350 endosomes being generated, but rather less DAF-16 on the vesicles which may be inconsistent
351 with these being signaling endosomes derived from DAF-2 internalization at the plasma
352 membrane. Future studies should test for additional IIS components on DAF-16 positive
353 endosomes.
354 If these are not signaling endosomes, then what are the DAF-16 endosomes? Since
355 RAB-5 and RAB-7 are also regulators of autophagy, so it is possible that these endosomes
356 contribute to degradation of inactive excess DAF-16. There is precedent for selective autophagy
357 in the degradation of the GATA4 transcription factor (Kang *et al.*, 2015). Alternatively, these
358 endosomes could serve as a reservoir of inactive DAF-16 that can be quickly mobilized if
359 environmental stress is encountered. For example, we found that acute starvation is a potent
360 regulator of DAF-16 endosome localization, even in the *tbc-2* mutant background.

361 We find it interesting that there is such variability within the population, and amongst the
362 intestinal cells in a given animal, as to whether there will be DAF-16 positive endosomes or not.
363 It suggests that each intestinal cell autonomously senses changes in IIS, or possibly other nutrient
364 and stress sensing pathways, to regulate DAF-16 localization. Then, why is endosomal DAF-16
365 more prominent in *tbc-2* mutants? One explaination would be that the expansion of endosomal
366 membranes in a *tbc-2* mutant create more storage space for inactive DAF-16. Another would be
367 that IIS or other pathways are more active in *tbc-2* mutants, or some combination of the two.
368

369 **A direct role for TBC-2 in regulating *daf-2(e1370) IGFR* mutant phenotypes**

370 Our finding that *tbc-2* was required for the extended lifespan and increased fat storage of *daf-*
371 *2(e1370)* mutants suggests that TBC-2 might have a more specific role related to IIS. However,
372 TBC-2 is not the first endosomal regulator required for lifespan extension of *daf-2(e1370)*
373 mutants. *C. elegans* BEC-1, a homolog of human Beclin1, is a regulator of autophagy and
374 endosome trafficking, and *bec-1* mutants accumulate large late endosomes in the intestinal cells
375 (Melendez *et al.*, 2003; Ruck *et al.*, 2011; Law *et al.*, 2017). Mutations in *bec-1* suppress the
376 increased lifespan of *daf-2(e1370)*, and were reported to be required for the increased fat storage
377 (Melendez *et al.*, 2003). Similarly, other autophagy regulators, *atg-7* and *atg-12*, have been
378 shown to be required for *daf-2* longevity (Hars *et al.*, 2007). An RNAi screen identified
379 regulators of endosome to lysosome trafficking, including RAB-7, and components of the
380 ESCRT and HOPS complexes as being required for the lifespan extension phenotypes of *daf-2*
381 *IGFR* mutants (Samuelson *et al.*, 2007). However, the mechanisms by which they regulate
382 lifespan are not known. In *daf-2(e1370)* mutants, there is an increase in autophagy and lysosome

383 function, both of which are required for the extended lifespan (Melendez *et al.*, 2003; Lapierre *et*
384 *al.*, 2013; Guo *et al.*, 2014; Sun *et al.*, 2020), consistent with increased stress resistance
385 contributing to increased longevity. Since the human homologs of TBC-2 are implicated in
386 autophagy (Behrends *et al.*, 2010; Popovic *et al.*, 2012; Carroll *et al.*, 2013; Toyofuku *et al.*,
387 2015), and *tbc-2* mutants accumulate autophagy protein LGG-1 (LC3/Atg8) in enlarged
388 endosomes (Chotard *et al.*, 2010a), it is possible that TBC-2 also regulates autophagy and thus
389 *daf-2(-)* longevity. However, our findings that TBC-2 regulates DAF-16 nuclear vs. endosome
390 localization and that TBC-2 is required for the DAF-16 target gene expression in *daf-2* mutants
391 demonstrate that TBC-2 has a more direct role in IIS, as opposed to being required for
392 downstream cellular responses. It will be interesting to test if TBC-2 regulates DAF-16-
393 independent mechanisms of longevity as well as to determine if other endosome and autophagy-
394 regulating genes can regulate DAF-16 localization to endosomes.
395
396 **FOXO localization to endosomes in human cells**
397 We demonstrated that FOXO proteins can localize to Rab5 and Rab7 endosomes in two
398 commonly used human cell lines, HeLa and HEK293. This localization was most prominent
399 with pFOXO1/3a, the inactive pool that is mostly excluded from the nucleus. Consistent with
400 our finding in *C. elegans* we found that siRNA knockdown of TBC1D2 and TBC1D2B increased
401 the endosomal localization of pFOXO1/3a and this effect was strongest with double knockdown,
402 indicating that TBC1D2 and TBC1D2B have overlapping functions. The increased endosomal
403 localization was accompanied by a decrease in nuclear FOXO3a and pFOXO1/3a. These data
404 suggest that the mechanisms in *C. elegans* are conserved in human cells. We did not detect

405 significant changes in protein expression levels or of the phosphorylation status of FOXO1 or
406 FOXO3a in TBC1D2 and TBC1D2B knockdown. This suggests that the TBC1D2 proteins do
407 not regulate FOXO expression or phosphorylation state. Given that Rab5 regulates IIS on
408 endosomes, further studies will be needed to determine if TBC1D2 and TBC1D2B functionally
409 impact IIS signaling outcomes in mammalian cells. Interestingly, TBC1D2 and TBC1D2B were
410 shown to interact with PI3,4,5P and that TBC1D2 was recruited to the plasma membrane upon
411 PDGFR/PI3K signal activation (Jungmichel *et al.*, 2014), suggesting the possibility of TBC1D2
412 and TBC1D2B regulation by IIS.

413 Endosomal localization of FOXO proteins is reminiscent of lysosomal regulation of the
414 TFEB family of transcription factors. Similar to FOXO, nuclear translocation of TFEB is
415 inhibited by phosphorylation and interactions with 14-3-3 proteins (Settembre *et al.*, 2013). In
416 this case, TFEB is phosphorylated by the nutrient sensing mTOR kinase on lysosomes.
417 Interestingly, the nuclear localization of *C. elegans* TFEB homolog, HLH-30, is inhibited by
418 DAF-2 IGFR and HLH-30 is required for the full lifespan extension of *daf-2(e1370)* mutants, as
419 well as lifespan extension by other perturbations and regulates fat storage (Lapierre *et al.*, 2013;
420 O'Rourke and Ruvkun, 2013). In fact HLH-30 and DAF-16 can interact in the nucleus to
421 combinatorially regulate expression of genes involved in longevity and oxidative stress
422 resistance (Lin *et al.*, 2018). We predict that regulators of endolysosomal trafficking, such as
423 TBC1D2 family of Rab GAPs, would perturb TFEB/HLH-30 regulation on lysosomes.
424

425 In conclusion, we demonstrate that DAF-16/FOXO transcription factors localize to
426 endosomes in *C. elegans* and in human cell lines. This endosomal localization of FOXO is
427 regulated by both IIS and the TBC-2 family of Rab5 and Rab7 GAPs. TBC-2/TBC1D2 promotes
428 the nuclear localization of DAF-16/FOXO, and in *C. elegans* this localization has functional
429 effects on both longevity and metabolism through modulation of DAF-16 target gene expression.
430 Our data suggest that endosomes serve as an important location for FOXO transcription factor
431 regulation, and suggest that endomembranes may function as a site of transcription factor
432 regulation.
433

434 **METHODS**

435 ***C. elegans* genetics and strain construction**

436 *C. elegans* strains were cultured as described in Wormbook (www.wormbook.org). The *C.*
437 *elegans* N2 Bristol strain was the wild-type parent strain and HB101 *E. coli* strain was used as a
438 food source. Both were obtained from the Caenorhabditis Genetic Center (CGC) as were many
439 of the strains used in this study (Table S1). New strains were constructed using standard
440 methods and the presence of mutations were confirmed by PCR and DNA sequencing.
441

442 **Cell culture and transfection**

443 HEK293 (CRL-1573) or HeLa (CCL-2) cells were obtained from the American Type Culture
444 Collection (ATCC; Manassas, VA). Cells were cultured in DMEM (Gibco, Grand Island, NY)
445 supplemented with 10% fetal bovine serum (FBS) and 1% penicillin/streptomycin (growth
446 medium) at 37°C with 5% CO2. Typically, cells were plated at a density (~150,000 cells/well in

447 a six-well plate) that would result in 70-75% confluence the following day, unless otherwise
448 noted.
449
450 **RNAi experiments**
451 *C. elegans* RNAi feeding experiments were conducted essentially as described in (Kamath *et al.*,
452 2001). The following RNAi feeding clones were obtained from the Ahringer RNAi library: *rab-*
453 *5* (I-4J01), *rab-7* (II-8G13), *akt-1* (V-7I17), *ftt-2* (X-5F07) and *par-5* (IV-6E06) and confirmed
454 by sequencing. The L4440 empty vector was used as a negative control (AddGene).
455 For siRNA transfection, HEK293 or HeLa cells at ∼70% confluence were transfected
456 with 25 nM oligonucleotides (IDT; Table S2) using JetPrime Reagent (Polyplus Transfection)
457 and following the manufacturer's protocol. The transfection mixture was replaced with fresh
458 growth medium the day following transfection and the cells were incubated for an additional 18-
459 24 hours before being harvested.
460
461 **Microscopy**
462 DAF-16 vesicular localization was analyzed in the intestinal cells of hermaphrodites.
463 Hermaphrodite worms at the L4 stage were imaged alive at room temperature unless it is stated
464 otherwise. Animals were picked and mounted onto 4% agarose pads, animals were anesthetized
465 with levamisole.
466 Differential interference contrast (DIC) and fluorescent imaging were performed with an
467 Axio Imager A1 compound microscope with a 100×1.3 NA Plan-Neofluar oil-immersion
468 objective lens (Zeiss) and images were captured by using an Axio Cam MRm camera and

469 AxioVision software (Zeiss). Confocal microscopy was performed on an Axio Observer Z1
470 LSM780 and LSM510 laser scanning confocal microscopes with a 63×1.4 NA Plan-Apochromat
471 oil-immersion objective lens (Zeiss) in a multi-track mode using an argon multiline laser (405
472 nm excitation for autofluoresence, 488 nm excitation for GFP and a 561/ 594 nm excitation for
473 mCherry/RFP). Images were captured with a 32 channel GaAsP detector and ZEN2010 image
474 software. Raw data was analyzed using Fiji (ImageJ) or Zen 2010 Lit programs, and images were
475 modified by using Fiji (ImageJ).

476 To compare DAF-16 (*zIs356*) nuclear intensity in cells with or without DAF-16 vesicles,
477 animals at L4 stage were imaged using an LSM780 scanning laser microscope. To ensure
478 consistency, only the anterior most intestine cells were imaged. First, the nucleus of intestinal
479 cells were focused under bright field and without changing the position, GFP, autofluoresence
480 and bright field signals were imaged. Each animal was imaged using the same confocal settings.
481 After data collection, each nucleus was categorized as a nucleus with adjacent DAF-16-positive
482 vesicles or a nucleus without any DAF-16 positive vesicles. Total GFP intensity inside the
483 nucleus was measured using Fiji (Image J) software. The nucleus is circled using DIC/Bright
484 Field and autofluorescence channels as reference. Since intestinal cells have two nuclei per cells,
485 if there are two nuclei within the focus, their GFP intensity is averaged for statistical analysis.
486 Prism 8 (GraphPad) were used to graph the data and determine statistical analysis using an
487 unpaired t-test.

488 HEK293 or HeLa cells (~60,000) were seeded on glass coverslips in 24-well plates and
489 incubated overnight in growth medium. The next day, cells were transfected with siRNA as
490 described under Cell culture and transfection. For immunofluorescence analysis, cells were

491 rinsed once in DMEM containing 10 mM HEPES and then fixed in 4% paraformaldehyde for 20
492 min. The cells were then rinsed twice in DMEM containing 10 mM HEPES, followed by a 1-h
493 incubation in DMEM containing 10 mM HEPES, 2% FBS, 0.1% Triton X-100, and primary
494 antibody (Table S3). Following three washes in DMEM containing 10 mM HEPES, the cells
495 were incubated for 1 h in DMEM containing 10 mM HEPES, 2% FBS, and fluorescently labeled
496 secondary antibody. The cells were washed three times, incubated for 10 min with 4′,6-
497 diamidino-2-phenylindole (DAPI) in PBS, rinsed two times with distilled water, and mounted on
498 glass slides using ProLong Gold anti-fade reagent (Life Technologies, Carlsbad, CA). Slides
499 were visualized as described using an Axio fluorescence microscope (40X or 63X magnification;
500 Zeiss, Oberkochen, Germany) and Zen imaging software.
501

502 **Starvation-Refeeding and Temperature Shift Experiments**

503 For starvation and refeeding experiments animals were synchronized at the L1 stage and grown
504 NGM plates with HB101 *E. coli* till the L4 stage. Then animals were collected washed 3 times
505 for 5 mins with M9 buffer to remove bacteria in their gut. After the third wash animals were
506 plated to regular NGM plates with or without HB101 *E. coli*, and incubated for 4-5 hours before
507 scoring. Animals are scored for the presence of DAF-16::GFP-positive vesicles the intestine
508 using an A1 Zeiss microscope. After 4h-5h of starvation, animals were harvested with M9 buffer
509 from the starved plates and washed once with M9 buffer and plated to NGM plates with HB101
510 *E. coli* and incubated for 1-2 hours at 20°C before scoring.
511

512 **Life span analysis**

513 Replicate strains were maintained for several generations prior to beginning the lifespan assays
514 which were conducted at 20°C. For each strain 25 young adult hermaphrodites were picked to
515 two NGM plates without FUDR seeded with HB101 *E. coli* for three independent replicates
516 totaling 150 animals. Strains were coded and scored blindly to reduce bias. Animals were
517 transferred to fresh NGM plates to avoid contamination and getting crowded out by their
518 progeny. Animals were scored every 2-3 days and were considered dead when they stop
519 exhibiting spontaneous movement and fail to move in response to 1) a gentle touch of the tail, 2)
520 a gentle touch of the head, and 3) gently lifting the head. Animals that die of unnatural causes
521 (internal hatching of embryos, bursting, or crawling off the plate) are omitted. Graphs and
522 statistics were done using Graphpad Prism. None of the strains used in the lifespan assays carry
523 the *fln-2(ot611)* mutation found in a N2 male stock strain and found to extend median lifespan
524 (Gems and Riddle, 2000; Zhao *et al.*, 2019).
525
526 **Fat staining**
527 L4 animals were fixed for staining with Nile Red (Invitrogen) or Oil Red O (Sigma-Aldrich) as
528 previously described (Escorcia *et al.*, 2018). Imaging and analysis was done as previously
529 described (Ratemi *et al.*, 2019). Graphs and statistics were done using Graphpad Prism.
530
531 **Quantitative real-time RT-PCR**
532 *C. elegans* RNA was isolated from young adults maintained at 15°C using TRIZOL reagent
533 (Invitrogen). RNA from HEK293 and HeLa cells was isolated by solubilizing cells in 4 M
534 guanidinium isothiocyanate and phenol-chloroform extraction. RNA concentration was

535 determined using a NanoDrop LITE spectrophotometer (Thermo Fisher Scientific). 1 ug of RNA
536 was reverse transcribed into cDNA using the High-Capacity cDNA Reverse Transcriptase Kit
537 (Applied Biosystems). Quantitative real-time PCR was performed using 1 µl of the cDNA
538 preparation with SYBR-Green Reagents and a Vii7 qPCR analyzer (Applied Biosystems). Each
539 DAF-16 target gene was amplified using PCR primers as described in (Senchuk *et al.*, 2018) and
540 compared to *act-3* (Table S4). TBC1D2 and TBC1D2B were compared to glyceraldehyde 3-
541 phosphate dehydrogenase (GAPDH) expression (Table S4).
542
543 **Statistical Analysis**
544 Statistical analysis was carried out using GraphPad Prism software. For the analysis of two
545 groups, a student t test was performed using two-tailed distribution for analysis involving two
546 groups of samples. Fishers' exact test was used for comparing groups of four. For each analysis,
547 $P<0.05$ was considered as significant.
548 For mammalian work: Student's t-test was used to compare the difference between two groups,
549 one-way analysis of variance (ANOVA) was used to compare the difference between three or
550 more groups, and two-way ANOVA was used to compare the difference between multiple
551 groups under different treatment conditions. A probability $P< 0.05$ was considered significant,
552 with specific values of significance provided the figure legends.
553
554
555
556 **ACKNOWLEDGEMENTS**

557 We thank Ali Fazlollahi for technical assistance, Meera Sundaram (University of Pennsylvania)
558 for comments and suggestions, Simon Wing, Richard Roy and Monique Zetka (McGill
559 University) for reagents, Aimee Kao (UCSF) for *muIs113*, as well as Yanping Zhang, Wenhong
560 Zhang and Meng-Qiu Dong (National Institute of Biological Sciences, Beijing) for generously
561 sharing *daf-16(hq23)* ahead of publication. Some strains were provided by the CGC, which is
562 funded by NIH Office of Research Infrastructure Programs (P40 OD010440). This work was
563 supported by a Canadian Institutes of Health Research (CIHR) Project Grant (PJT-159725) and
564 in part from the RI-MUHC which receives funding from the Fonds de Recherche du Quebec
565 Santé (FRQS). JVR is supported by the CIHR, the Natural Sciences and Engineering Research
566 Council of Canada (NSERC) and the National Institute of General Medical Sciences (NIGMS;
567 Grant number R01 GM121756). JVR received a salary award from the FRQS. TL received a
568 scholarship from FRQS.
569

570 **REFERENCES**

571

572 Accili D, Arden KC (2004). FoxOs at the crossroads of cellular metabolism, differentiation, and
573 transformation. Cell *117*, 421-426.

574 Ackerman D, Gems D (2012). Insulin/IGF-1 and hypoxia signaling act in concert to regulate iron
575 homeostasis in Caenorhabditis elegans. PLoS Genet *8*, e1002498.

576 Baass PC, Di Guglielmo GM, Authier F, Posner BI, Bergeron JJ (1995). Compartmentalized
577 signal transduction by receptor tyrosine kinases. Trends Cell Biol *5*, 465-470.

578 Balbis A, Baquiran G, Bergeron JJ, Posner BI (2000). Compartmentalization and insulin-induced
579 translocations of insulin receptor substrates, phosphatidylinositol 3-kinase, and protein kinase B
580 in rat liver. Endocrinology *141*, 4041-4049.

581 Barthel A, Schmoll D, Unterman TG (2005). FoxO proteins in insulin action and metabolism.
582 Trends Endocrinol Metab *16*, 183-189.

583 Baugh LR, Sternberg PW (2006). DAF-16/FOXO regulates transcription of cki-1/Cip/Kip and
584 repression of lin-4 during C. elegans L1 arrest. Curr Biol *16*, 780-785.

585 Behrends C, Sowa ME, Gygi SP, Harper JW (2010). Network organization of the human
586 autophagy system. Nature *466*, 68-76.

587 Bergeron JJ, Di Guglielmo GM, Dahan S, Dominguez M, Posner BI (2016). Spatial and
588 Temporal Regulation of Receptor Tyrosine Kinase Activation and Intracellular Signal
589 Transduction. Annual review of biochemistry *85*, 573-597.

590 Braccini L, Ciraolo E, Campa CC, Perino A, Longo DL, Tibolla G, Pregnolato M, Cao Y,
591 Tassone B, Damilano F*, et al.* (2015). PI3K-C2gamma is a Rab5 effector selectively controlling
592 endosomal Akt2 activation downstream of insulin signalling. Nature communications *6*, 7400.

593 Brunet A, Bonni A, Zigmond MJ, Lin MZ, Juo P, Hu LS, Anderson MJ, Arden KC, Blenis J,
594 Greenberg ME (1999). Akt promotes cell survival by phosphorylating and inhibiting a Forkhead
595 transcription factor. Cell *96*, 857-868.
596 Carroll B, Mohd-Naim N, Maximiano F, Frasa MA, McCormack J, Finelli M, Thoresen SB,
597 Perdios L, Daigaku R, Francis RE*, et al.* (2013). The TBC/RabGAP Armus coordinates Rac1
598 and Rab7 functions during autophagy. Dev Cell *25*, 15-28.
599 Chavrier P, Parton RG, Hauri HP, Simons K, Zerial M (1990). Localization of low molecular
600 weight GTP binding proteins to exocytic and endocytic compartments. Cell *62*, 317-329.
601 Chen CC, Schweinsberg PJ, Vashist S, Mareiniss DP, Lambie EJ, Grant BD (2006). RAB-10 Is
602 Required for Endocytic Recycling in the Caenorhabditis elegans Intestine. Mol Biol Cell *17*,
603 1286-1297.
604 Cheng KK, Iglesias MA, Lam KS, Wang Y, Sweeney G, Zhu W, Vanhoutte PM, Kraegen EW,
605 Xu A (2009). APPL1 potentiates insulin-mediated inhibition of hepatic glucose production and
606 alleviates diabetes via Akt activation in mice. Cell Metab *9*, 417-427.
607 Chotard L, Mishra AK, Sylvain MA, Tuck S, Lambright DG, Rocheleau CE (2010a). TBC-2
608 regulates RAB-5/RAB-7-mediated endosomal trafficking in Caenorhabditis elegans. Mol Biol
609 Cell *21*, 2285-2296.
610 Chotard L, Skorobogata O, Sylvain MA, Shrivastava S, Rocheleau CE (2010b). TBC-2 is
611 required for embryonic yolk protein storage and larval survival during L1 diapause in
612 Caenorhabditis elegans. PLoS One *5*, e15662.
613 Christoforidis S, Miaczynska M, Ashman K, Wilm M, Zhao L, Yip SC, Waterfield MD, Backer
614 JM, Zerial M (1999). Phosphatidylinositol-3-OH kinases are Rab5 effectors. Nat Cell Biol *1*,
615 249-252.

616 Clokey GV, Jacobson LA (1986). The autofluorescent "lipofuscin granules" in the intestinal cells
617 of Caenorhabditis elegans are secondary lysosomes. Mech Ageing Dev *35*, 79-94.
618 Escorcia W, Ruter DL, Nhan J, Curran SP (2018). Quantification of Lipid Abundance and
619 Evaluation of Lipid Distribution in Caenorhabditis elegans by Nile Red and Oil Red O Staining.
620 J Vis Exp.
621 Frasa MA, Maximiano FC, Smolarczyk K, Francis RE, Betson ME, Lozano E, Goldenring J,
622 Seabra MC, Rak A, Ahmadian MR*, et al.* (2010). Armus is a Rac1 effector that inactivates Rab7
623 and regulates E-cadherin degradation. Curr Biol *20*, 198-208.
624 Gems D, Riddle DL (2000). Defining wild-type life span in Caenorhabditis elegans. J Gerontol
625 A Biol Sci Med Sci *55*, B215-219.
626 Greer EL, Brunet A (2005). FOXO transcription factors at the interface between longevity and
627 tumor suppression. Oncogene *24*, 7410-7425.
628 Guo B, Huang X, Zhang P, Qi L, Liang Q, Zhang X, Huang J, Fang B, Hou W, Han J*, et al.*
629 (2014). Genome-wide screen identifies signaling pathways that regulate autophagy during
630 Caenorhabditis elegans development. EMBO Rep *15*, 705-713.
631 Harms FL, Parthasarathy P, Zorndt D, Alawi M, Fuchs S, Halliday BJ, McKeown C, Sampaio H,
632 Radhakrishnan N, Radhakrishnan SK*, et al.* (2020). Biallelic loss-of-function variants in
633 TBC1D2B cause a neurodevelopmental disorder with seizures and gingival overgrowth. Hum
634 Mutat *41*, 1645-1661.
635 Hars ES, Qi H, Ryazanov AG, Jin S, Cai L, Hu C, Liu LF (2007). Autophagy regulates ageing in
636 C. elegans. Autophagy *3*, 93-95.
637 Henderson ST, Johnson TE (2001). daf-16 integrates developmental and environmental inputs to
638 mediate aging in the nematode Caenorhabditis elegans. Curr Biol *11*, 1975-1980.

639 Hertweck M, Gobel C, Baumeister R (2004). C. elegans SGK-1 is the critical component in the
640 Akt/PKB kinase complex to control stress response and life span. Dev Cell *6*, 577-588.
641 Honda Y, Honda S (1999). The daf-2 gene network for longevity regulates oxidative stress
642 resistance and Mn-superoxide dismutase gene expression in Caenorhabditis elegans. FASEB
643 journal : official publication of the Federation of American Societies for Experimental Biology
644 *13*, 1385-1393.
645 Hsu JW, Bai M, Li K, Yang JS, Chu N, Cole PA, Eck MJ, Li J, Hsu VW (2020). The protein
646 kinase Akt acts as a coat adaptor in endocytic recycling. Nat Cell Biol *22*, 927-933.
647 Huotari J, Helenius A (2011). Endosome maturation. EMBO J *30*, 3481-3500.
648 Jaber N, Mohd-Naim N, Wang Z, DeLeon JL, Kim S, Zhong H, Sheshadri N, Dou Z, Edinger
649 AL, Du G*, et al.* (2016). Vps34 regulates Rab7 and late endocytic trafficking through recruitment
650 of the GTPase-activating protein Armus. J Cell Sci *129*, 4424-4435.
651 Jungmichel S, Sylvestersen KB, Choudhary C, Nguyen S, Mann M, Nielsen ML (2014).
652 Specificity and commonality of the phosphoinositide-binding proteome analyzed by quantitative
653 mass spectrometry. Cell Rep *6*, 578-591.
654 Kamath RS, Martinez-Campos M, Zipperlen P, Fraser AG, Ahringer J (2001). Effectiveness of
655 specific RNA-mediated interference through ingested double-stranded RNA in Caenorhabditis
656 elegans. Genome Biol *2*, RESEARCH0002.
657 Kang C, Xu Q, Martin TD, Li MZ, Demaria M, Aron L, Lu T, Yankner BA, Campisi J, Elledge
658 SJ (2015). The DNA damage response induces inflammation and senescence by inhibiting
659 autophagy of GATA4. Science *349*, aaa5612.

660 Kanno E, Ishibashi K, Kobayashi H, Matsui T, Ohbayashi N, Fukuda M (2010). Comprehensive
661 screening for novel rab-binding proteins by GST pull-down assay using 60 different mammalian
662 Rabs. Traffic *11*, 491-507.
663 Kenyon C, Chang J, Gensch E, Rudner A, Tabtiang R (1993). A C. elegans mutant that lives
664 twice as long as wild type. Nature *366*, 461-464.
665 Khan MN, Savoie S, Bergeron JJ, Posner BI (1986). Characterization of rat liver endosomal
666 fractions. In vivo activation of insulin-stimulable receptor kinase in these structures. J Biol Chem
667 *261*, 8462-8472.
668 Kim Y, Shiba-Ishii A, Nakagawa T, Iemura SI, Natsume T, Nakano N, Matsuoka R, Sakashita S,
669 Lee S, Kawaguchi A*, et al.* (2018). Stratifin regulates stabilization of receptor tyrosine kinases
670 via interaction with ubiquitin-specific protease 8 in lung adenocarcinoma. Oncogene *37*, 5387-
671 5402.
672 Kimura KD, Tissenbaum HA, Liu Y, Ruvkun G (1997). daf-2, an insulin receptor-like gene that
673 regulates longevity and diapause in Caenorhabditis elegans. Science *277*, 942-946.
674 Kwon ES, Narasimhan SD, Yen K, Tissenbaum HA (2010). A new DAF-16 isoform regulates
675 longevity. Nature *466*, 498-502.
676 Lapierre LR, De Magalhaes Filho CD, McQuary PR, Chu CC, Visvikis O, Chang JT, Gelino S,
677 Ong B, Davis AE, Irazoqui JE*, et al.* (2013). The TFEB orthologue HLH-30 regulates autophagy
678 and modulates longevity in Caenorhabditis elegans. Nature communications *4*, 2267.
679 Law F, Seo JH, Wang Z, DeLeon JL, Bolis Y, Brown A, Zong WX, Du G, Rocheleau CE
680 (2017). The VPS34 PI3K negatively regulates RAB-5 during endosome maturation. J Cell Sci
681 *130*, 2007-2017.

682 Li W, Zou W, Zhao D, Yan J, Zhu Z, Lu J, Wang X (2009). C. elegans Rab GTPase activating
683 protein TBC-2 promotes cell corpse degradation by regulating the small GTPase RAB-5.
684 Development *136*, 2445-2455.
685 Libina N, Berman JR, Kenyon C (2003). Tissue-specific activities of C. elegans DAF-16 in the
686 regulation of lifespan. Cell *115*, 489-502.
687 Lin K, Dorman JB, Rodan A, Kenyon C (1997). daf-16: An HNF-3/forkhead family member that
688 can function to double the life-span of Caenorhabditis elegans. Science *278*, 1319-1322.
689 Lin K, Hsin H, Libina N, Kenyon C (2001). Regulation of the Caenorhabditis elegans longevity
690 protein DAF-16 by insulin/IGF-1 and germline signaling. Nat Genet *28*, 139-145.
691 Lin XX, Sen I, Janssens GE, Zhou X, Fonslow BR, Edgar D, Stroustrup N, Swoboda P, Yates
692 JR, 3rd, Ruvkun G*, et al.* (2018). DAF-16/FOXO and HLH-30/TFEB function as combinatorial
693 transcription factors to promote stress resistance and longevity. Nature communications *9*, 4400.
694 Liu O, Grant BD (2015). Basolateral Endocytic Recycling Requires RAB-10 and AMPH-1
695 Mediated Recruitment of RAB-5 GAP TBC-2 to Endosomes. PLoS Genet *11*, e1005514.
696 Manshouri R, Coyaud E, Kundu ST, Peng DH, Stratton SA, Alton K, Bajaj R, Fradette JJ,
697 Minelli R, Peoples MD*, et al.* (2019). ZEB1/NuRD complex suppresses TBC1D2b to stimulate
698 E-cadherin internalization and promote metastasis in lung cancer. Nature communications *10*,
699 5125.
700 Marat AL, Wallroth A, Lo WT, Muller R, Norata GD, Falasca M, Schultz C, Haucke V (2017).
701 mTORC1 activity repression by late endosomal phosphatidylinositol 3,4-bisphosphate. Science
702 *356*, 968-972.

703 Melendez A, Talloczy Z, Seaman M, Eskelinen EL, Hall DH, Levine B (2003). Autophagy genes
704 are essential for dauer development and life-span extension in C. elegans. Science *301*, 1387-
705 1391.
706 Miaczynska M (2013). Effects of membrane trafficking on signaling by receptor tyrosine
707 kinases. Cold Spring Harbor perspectives in biology *5*, a009035.
708 Mondin VE, Ben El Kadhi K, Cauvin C, Jackson-Crawford A, Belanger E, Decelle B, Salomon
709 R, Lowe M, Echard A, Carreno S (2019). PTEN reduces endosomal PtdIns(4,5)P2 in a
710 phosphatase-independent manner via a PLC pathway. J Cell Biol *218*, 2198-2214.
711 Morton DG, Shakes DC, Nugent S, Dichoso D, Wang W, Golden A, Kemphues KJ (2002). The
712 Caenorhabditis elegans par-5 gene encodes a 14-3-3 protein required for cellular asymmetry in
713 the early embryo. Dev Biol *241*, 47-58.
714 Munoz MJ, Riddle DL (2003). Positive selection of Caenorhabditis elegans mutants with
715 increased stress resistance and longevity. Genetics *163*, 171-180.
716 Murphy CT, Hu PJ (2013). Insulin/insulin-like growth factor signaling in C. elegans.
717 WormBook, 1-43.
718 Murphy CT, McCarroll SA, Bargmann CI, Fraser A, Kamath RS, Ahringer J, Li H, Kenyon C
719 (2003). Genes that act downstream of DAF-16 to influence the lifespan of Caenorhabditis
720 elegans. Nature *424*, 277-283.
721 Naguib A, Bencze G, Cho H, Zheng W, Tocilj A, Elkayam E, Faehnle CR, Jaber N, Pratt CP,
722 Chen M*, et al.* (2015). PTEN functions by recruitment to cytoplasmic vesicles. Mol Cell *58*, 255-
723 268.
724 O'Rourke EJ, Ruvkun G (2013). MXL-3 and HLH-30 transcriptionally link lipolysis and
725 autophagy to nutrient availability. Nat Cell Biol *15*, 668-676.

726 O'Rourke EJ, Soukas AA, Carr CE, Ruvkun G (2009). C. elegans major fats are stored in
727 vesicles distinct from lysosome-related organelles. Cell Metab *10*, 430-435.
728 Ogg S, Paradis S, Gottlieb S, Patterson GI, Lee L, Tissenbaum HA, Ruvkun G (1997). The Fork
729 head transcription factor DAF-16 transduces insulin-like metabolic and longevity signals in C.
730 elegans. Nature *389*, 994-999.
731 Ogg S, Ruvkun G (1998). The C. elegans PTEN homolog, DAF-18, acts in the insulin receptor-
732 like metabolic signaling pathway. Mol Cell *2*, 887-893.
733 Paradis S, Ruvkun G (1998). Caenorhabditis elegans Akt/PKB transduces insulin receptor-like
734 signals from AGE-1 PI3 kinase to the DAF-16 transcription factor. Genes Dev *12*, 2488-2498.
735 Popovic D, Akutsu M, Novak I, Harper JW, Behrends C, Dikic I (2012). Rab GTPase-activating
736 proteins in autophagy: regulation of endocytic and autophagy pathways by direct binding to
737 human ATG8 modifiers. Mol Cell Biol *32*, 1733-1744.
738 Ratemi Z, Kiss R, Rocheleau C (2019). C. elegans rab-18 mutants display reduced lipid content
739 under fed and fasted conditions. MicroPubl Biol *2019*.
740 Riddle DL, Swanson MM, Albert PS (1981). Interacting genes in nematode dauer larva
741 formation. Nature *290*, 668-671.
742 Ruck A, Attonito J, Garces KT, Nunez L, Palmisano NJ, Rubel Z, Bai Z, Nguyen KC, Sun L,
743 Grant BD*, et al.* (2011). The Atg6/Vps30/Beclin 1 ortholog BEC-1 mediates endocytic
744 retrograde transport in addition to autophagy in C. elegans. Autophagy *7*, 386-400.
745 Samuelson AV, Carr CE, Ruvkun G (2007). Gene activities that mediate increased life span of
746 C. elegans insulin-like signaling mutants. Genes Dev *21*, 2976-2994.

747 Sasidharan N, Sumakovic M, Hannemann M, Hegermann J, Liewald JF, Olendrowitz C, Koenig
748 S, Grant BD, Rizzoli SO, Gottschalk A*, et al.* (2012). RAB-5 and RAB-10 cooperate to regulate
749 neuropeptide release in Caenorhabditis elegans. Proc Natl Acad Sci U S A *109*, 18944-18949.
750 Sato M, Sato K, Fonarev P, Huang CJ, Liou W, Grant BD (2005). Caenorhabditis elegans RME-
751 6 is a novel regulator of RAB-5 at the clathrin-coated pit. Nat Cell Biol *7*, 559-569.
752 Schenck A, Goto-Silva L, Collinet C, Rhinn M, Giner A, Habermann B, Brand M, Zerial M
753 (2008). The endosomal protein Appl1 mediates Akt substrate specificity and cell survival in
754 vertebrate development. Cell *133*, 486-497.
755 Senchuk MM, Dues DJ, Schaar CE, Johnson BK, Madaj ZB, Bowman MJ, Winn ME, Van
756 Raamsdonk JM (2018). Activation of DAF-16/FOXO by reactive oxygen species contributes to
757 longevity in long-lived mitochondrial mutants in Caenorhabditis elegans. PLoS Genet *14*,
758 e1007268.
759 Serva A, Knapp B, Tsai YT, Claas C, Lisauskas T, Matula P, Harder N, Kaderali L, Rohr K,
760 Erfle H*, et al.* (2012). miR-17-5p regulates endocytic trafficking through targeting
761 TBC1D2/Armus. PLoS One *7*, e52555.
762 Settembre C, Fraldi A, Medina DL, Ballabio A (2013). Signals from the lysosome: a control
763 centre for cellular clearance and energy metabolism. Nat Rev Mol Cell Biol *14*, 283-296.
764 Shin HW, Hayashi M, Christoforidis S, Lacas-Gervais S, Hoepfner S, Wenk MR, Modregger J,
765 Uttenweiler-Joseph S, Wilm M, Nystuen A*, et al.* (2005). An enzymatic cascade of Rab5
766 effectors regulates phosphoinositide turnover in the endocytic pathway. J Cell Biol *170*, 607-618.
767 Shinde SR, Maddika S (2016). PTEN modulates EGFR late endocytic trafficking and
768 degradation by dephosphorylating Rab7. Nature communications *7*, 10689.

769 Shinde SR, Maddika S (2017). PTEN Regulates Glucose Transporter Recycling by Impairing
770 SNX27 Retromer Assembly. Cell Rep *21*, 1655-1666.
771 Su X, Lodhi IJ, Saltiel AR, Stahl PD (2006). Insulin-stimulated Interaction between insulin
772 receptor substrate 1 and p85alpha and activation of protein kinase B/Akt require Rab5. J Biol
773 Chem *281*, 27982-27990.
774 Sun L, Liu O, Desai J, Karbassi F, Sylvain MA, Shi A, Zhou Z, Rocheleau CE, Grant BD
775 (2012). CED-10/Rac1 regulates endocytic recycling through the RAB-5 GAP TBC-2. PLoS
776 Genet *8*, e1002785.
777 Sun Y, Li M, Zhao D, Li X, Yang C, Wang X (2020). Lysosome activity is modulated by
778 multiple longevity pathways and is important for lifespan extension in C. elegans. Elife *9*.
779 Swanson MM, Riddle DL (1981). Critical periods in the development of the Caenorhabditis
780 elegans dauer larva. Dev Biol *84*, 27-40.
781 Tepper RG, Ashraf J, Kaletsky R, Kleemann G, Murphy CT, Bussemaker HJ (2013). PQM-1
782 complements DAF-16 as a key transcriptional regulator of DAF-2-mediated development and
783 longevity. Cell *154*, 676-690.
784 Toyofuku T, Morimoto K, Sasawatari S, Kumanogoh A (2015). Leucine-Rich Repeat Kinase 1
785 Regulates Autophagy through Turning On TBC1D2-Dependent Rab7 Inactivation. Mol Cell Biol
786 *35*, 3044-3058.
787 Walz HA, Shi X, Chouinard M, Bue CA, Navaroli DM, Hayakawa A, Zhou QL, Nadler J,
788 Leonard DM, Corvera S (2010). Isoform-specific regulation of Akt signaling by the endosomal
789 protein WDFY2. J Biol Chem *285*, 14101-14108.
790 Wang W, Shakes DC (1997). Expression patterns and transcript processing of ftt-1 and ftt-2, two
791 C. elegans 14-3-3 homologues. J Mol Biol *268*, 619-630.

792 Wang Y, Oh SW, Deplancke B, Luo J, Walhout AJ, Tissenbaum HA (2006). C. elegans 14-3-3
793 proteins regulate life span and interact with SIR-2.1 and DAF-16/FOXO. Mech Ageing Dev *127*,
794 741-747.
795 Wei D, Zhan W, Gao Y, Huang L, Gong R, Wang W, Zhang R, Wu Y, Gao S, Kang T (2021).
796 RAB31 marks and controls an ESCRT-independent exosome pathway. Cell Res *31*, 157-177.
797 Zeigerer A, Bogorad RL, Sharma K, Gilleron J, Seifert S, Sales S, Berndt N, Bulik S, Marsico G,
798 D'Souza RCJ*, et al.* (2015). Regulation of liver metabolism by the endosomal GTPase Rab5. Cell
799 Rep *11*, 884-892.
800 Zhao Y, Wang H, Poole RJ, Gems D (2019). A fln-2 mutation affects lethal pathology and
801 lifespan in C. elegans. Nature communications *10*, 5087.
802
803

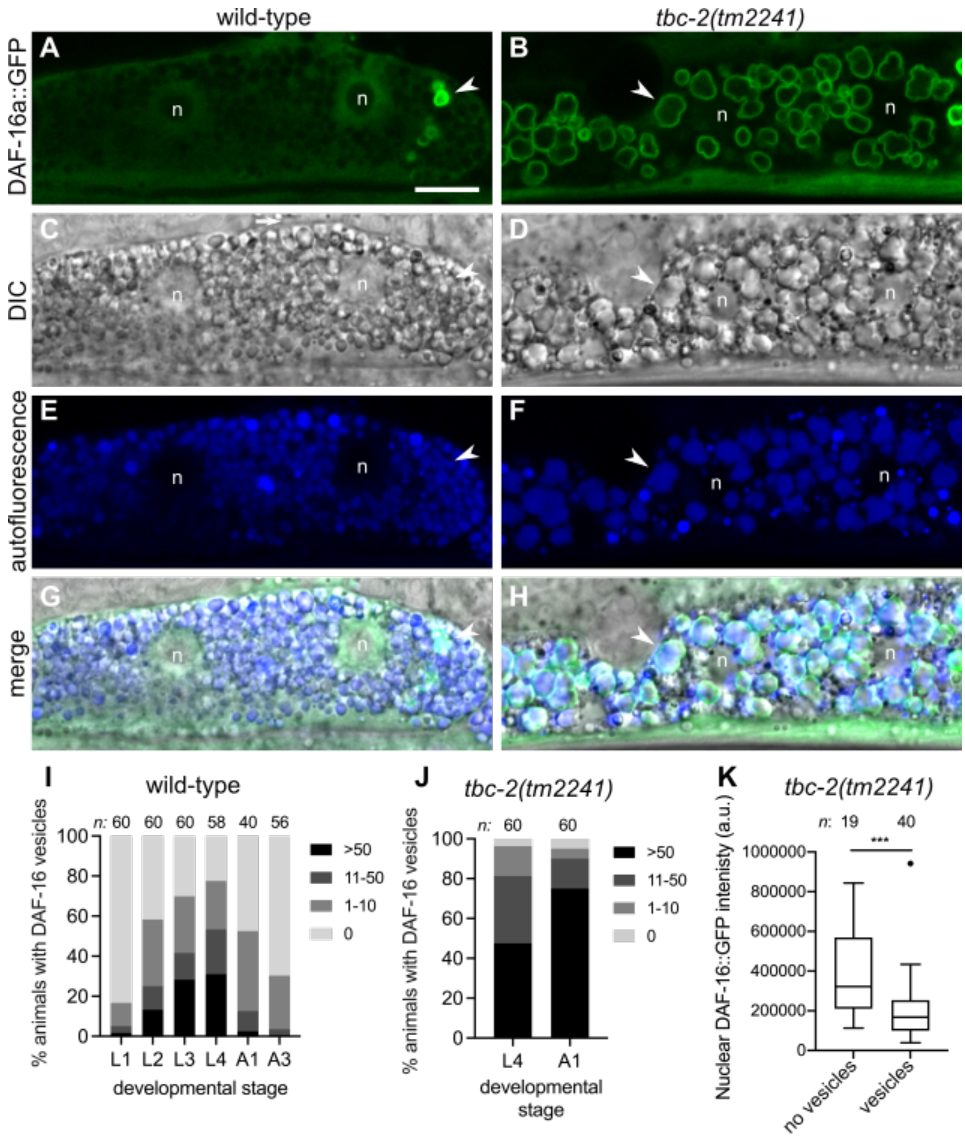

Figure 1. DAF-16 FOXO localizes to vesicles in intestinal cells

(A-H) Representative confocal and differential interference contrast (DIC) images of an intestinal cell of wild-type (A, C, E, G) and *tbc-2(tm2241)* (B, D, F, H) animals expressing DAF-16a::GFP *(zIs356)*. DAF-16a::GFP (green) is present on vesicles in both wild-type and *tbc-2(tm2241)* intestinal cells (A and B) that are positive for autofluorescence (blue) present in the the endolysosomal system (E and F). Corresponding DIC (C and D) and merged (G and F) images are shown. A representative vesicle is shown (arrow head) and the two nuclei of the binucleate cell are marked (n). Note that DAF-16a::GFP is excluded from the large nucleoli (A).

812 (I-J) Grouped bar graphs quantifying the percentage of wild-type (I) and *tbc-2(tm2241)* (J)
813 animals with 0, 1-10, 11-50 or >50 DAF-16a::GFP *(zIs356)* positive vesicles at the different
814 larval stages (L1-4) or 1 and 3 day old adults (A1 and A3). (K) A Tukey boxplot of the nuclear
815 intensity in artificial units (a.u.) of DAF-16a::GFP in *tbc-2(tm2241)* intestinal cells with and
816 without DAF-16a::GFP positive vesicles. *n,* total number of animals *** *P<0.001* in an unpaired
817 t test (Prism 8). Scale bar (A), 10µm.

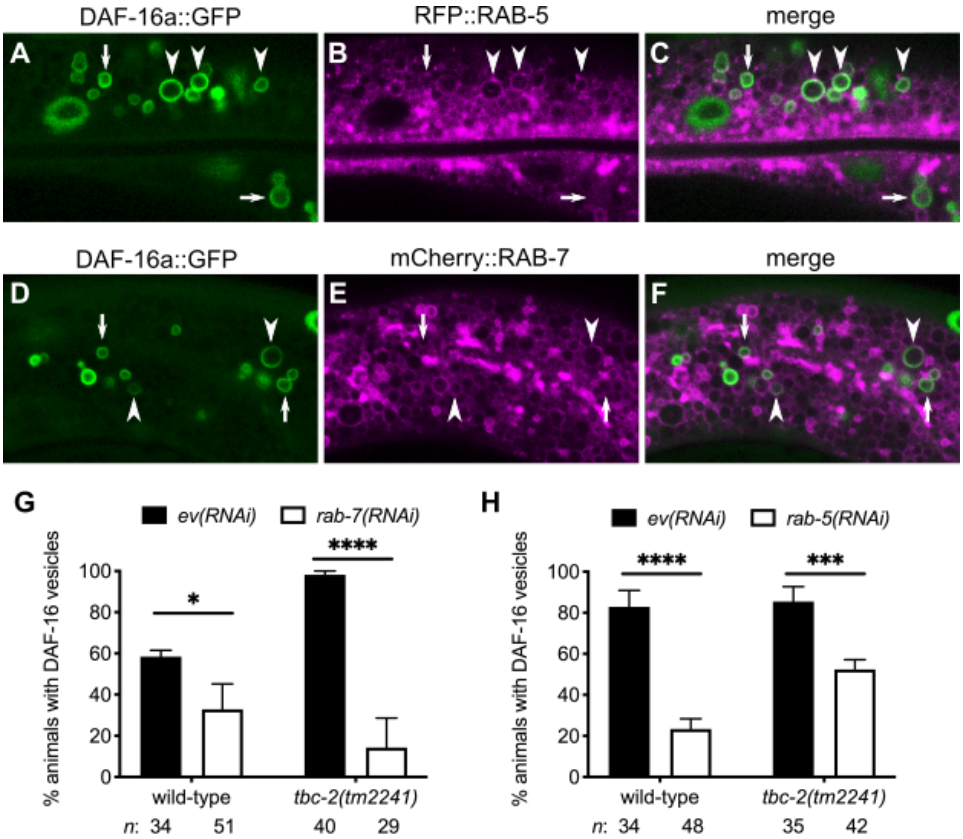

818

819 **Figure 2. RAB-5 and RAB-7 GTPases promote DAF-16 FOXO localization to endosomes**
820 (A-F) Representative confocal images of the intestinal cells of animals expressing DAF-
821 16a::GFP (*zIs356)* (green) and either RFP::RAB-5 (*pwIs480*) (A-C) or mCherry::RAB-7
822 (*pwIs429*) (magenta) (D- F). Arrowheads mark examples of vesicles positive for both DAF-
823 16a::GFP and either RFP::RAB-5 or mCherry::RAB-7. Arrows mark examples of DAF-

824 16a::GFP vesicles that are not positive for either RFP::RAB-5 or mCherry::RAB-7. (G and H)
825 Bar graphs displaying the mean (and SEM) of the percent wild-type and *tbc-2(tm2241)* animals
826 with DAF-16a::GFP (*zIs356*) vesicles fed bacteria expressing control empty vector (ev) RNAi
827 (black bars) compared to animals fed *rab-5(RNAi)* or *rab-7(RNAi)* (white bars) from three
828 independent experiments. Fisher's exact test (graphpad.com) was used to determine the
829 statistical difference between conditions. *n*, total number of animals. * $P<0.05$, *** $P<0.001$,
830 **** $P<0.0001$.

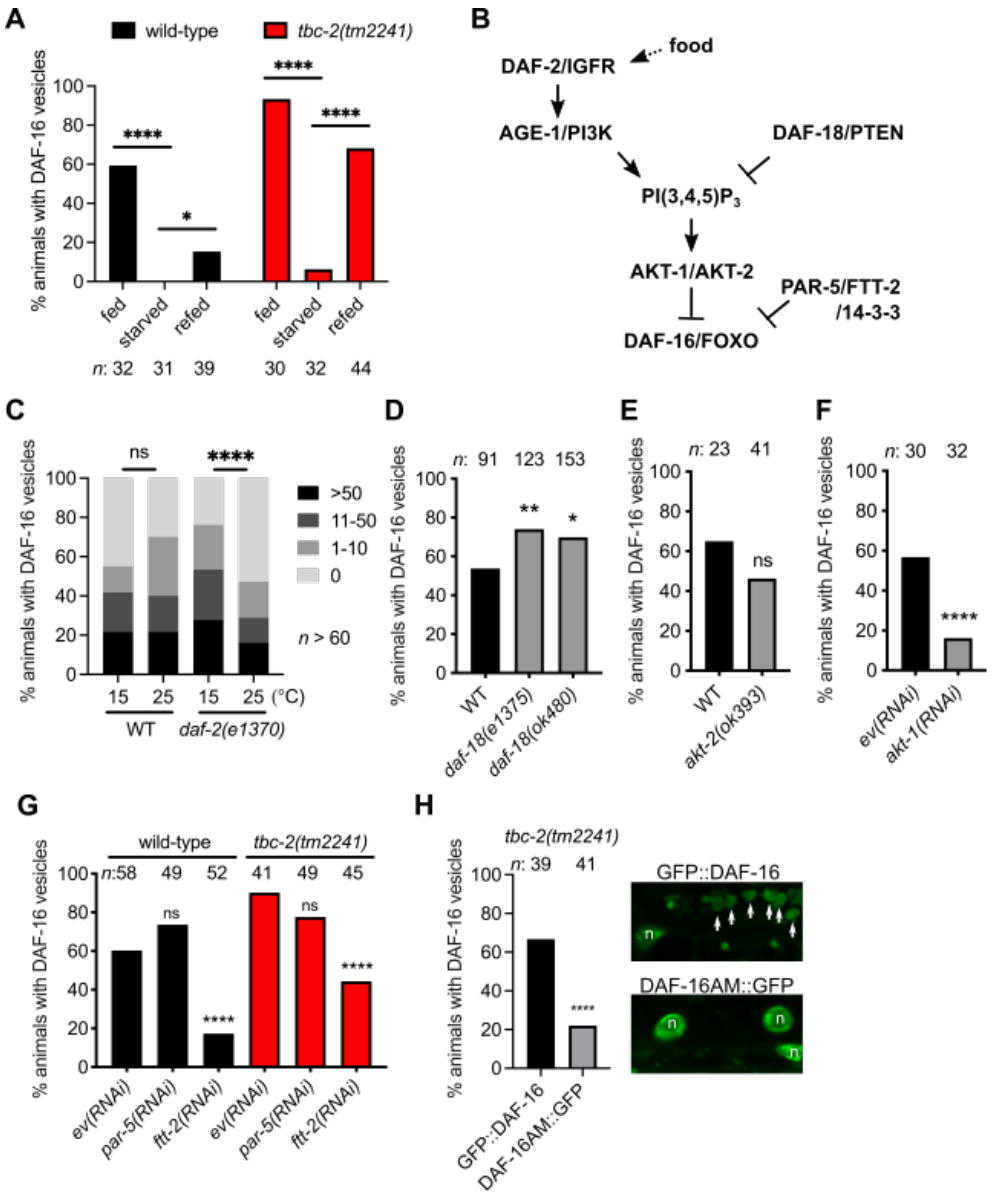

Figure 3. DAF-16 FOXO endosome localization is regulated by IIS and nutrient availability

(A) Bar graphs of the percent wild-type (black) and *tbc-2(tm2241)* (red) animals with DAF-16a::GFP (*zIs356*) vesicles in fed animals, animals starved between 4 and 5 hours and starved animals that have been refed for 1 to 2 hours. (B) Diagram of IIS-mediate regulation of DAF-16/FOXO. (C) Grouped bar graphs quantifying the percentage of wild-type and *daf-2(e1370)* L4 larvae (cumulative data from 3 independent strains) with 0, 1-10, 11-50 or >50 DAF-16a::GFP

838 *(zIs356)* positive vesicles at 15°C or shifted overnight to 25°C. (D) Bar graphs of percent wild-
839 type (black) and *daf-18(e1375)* (gray, 3 independent strains) and *daf-18(ok480)* (gray, 5
840 independent strains) with DAF-16a::GFP (*zIs356*) vesicles. (E) Bar graphs of percent wild-type
841 (black) and *akt-2(ok393)* (gray, 2 independent strains). (F) Bar graphs of percent wild-type
842 animals treated with control empty vector RNAi (black) and *akt-1(RNAi)* (gray). (G) Bar graphs
843 of the percent wild-type (black) and *tbc-2(tm2241)* (red) animals fed control empty vector RNAi,
844 *par-5(RNAi)* and *ftt-2(RNAi)* with DAF-16a::GFP (*zIs356*) vesicles. (H) Bar graph of the precent
845 *tbc-2(tm2241)* animals with GFP::DAF-16a (*muIs71*) or DAF-16a^{AM}::GFP *(muIs113)*-positive
846 vesicles. Representative images of GFP::DAF-16a (*muIs71*) (top) and DAF-16a^{AM}::GFP
847 *(muIs113)* (bottom) are shown. GFP::DAF-16a vesicles (arrows) and the nuclei (n). Fisher's
848 exact test (graphpad.com) was used to determine the statistical difference between conditions. *n*,
849 total number of animals. ns, not significant, * $P<0.05$, ** $P<0.01$, **** $P<0.0001$.
850
851
852
853

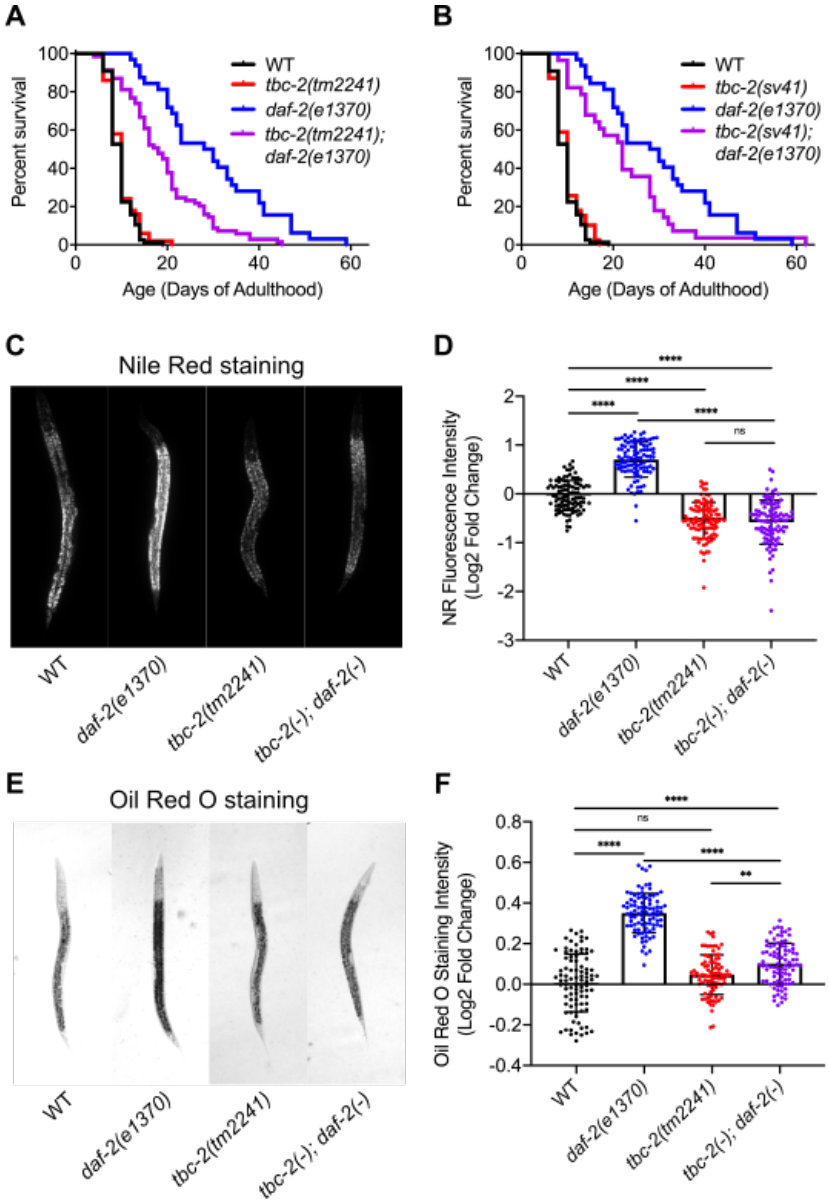

854 **Figure 4. TBC-2 is required for full lifespan extension and increased fat storage resulting**

855 **from decreased insulin/IGF signaling**

856 (A,B) Percent survival curve of adult animals of wild-type and *daf-2(e1370)* with either *tbc-*

857 *2(tm2241)* and *tbc-2(tm2241); daf-2(e1370)* (A) or *tbc-2(sv41)* and *tbc-2(sv41); daf-2(e1370)*

858 (B) genotypes. The survival of all strains are statistically different from *daf-2(e1370)* animals

859 ($P<0.001$) with the exception of *tbc-2(sv41); daf-2(e1370)* ($P=0.0314$) as determined by a

860 Mantel-Cox log-rank test. Cumulative data from three independent replicates of 50 young adults

861 for a total of 150. (C,D) Log2 fold change in Nile Red (NR) fluorescence intensity (C) or Oil
862 Red O staining intensity (D) comparing wild-type, *daf-2(e1370)*, *tbc-2(tm2241)* and *tbc-*
863 *2(tm2241); daf-2(e1370)* fixed L4 hermaphrodites. Statistical analysis was done using a
864 student's t-test with a one way analysis of variance (ANOVA). ns, not significant. ** P <0.01,
865 **** P <0.0001.
866

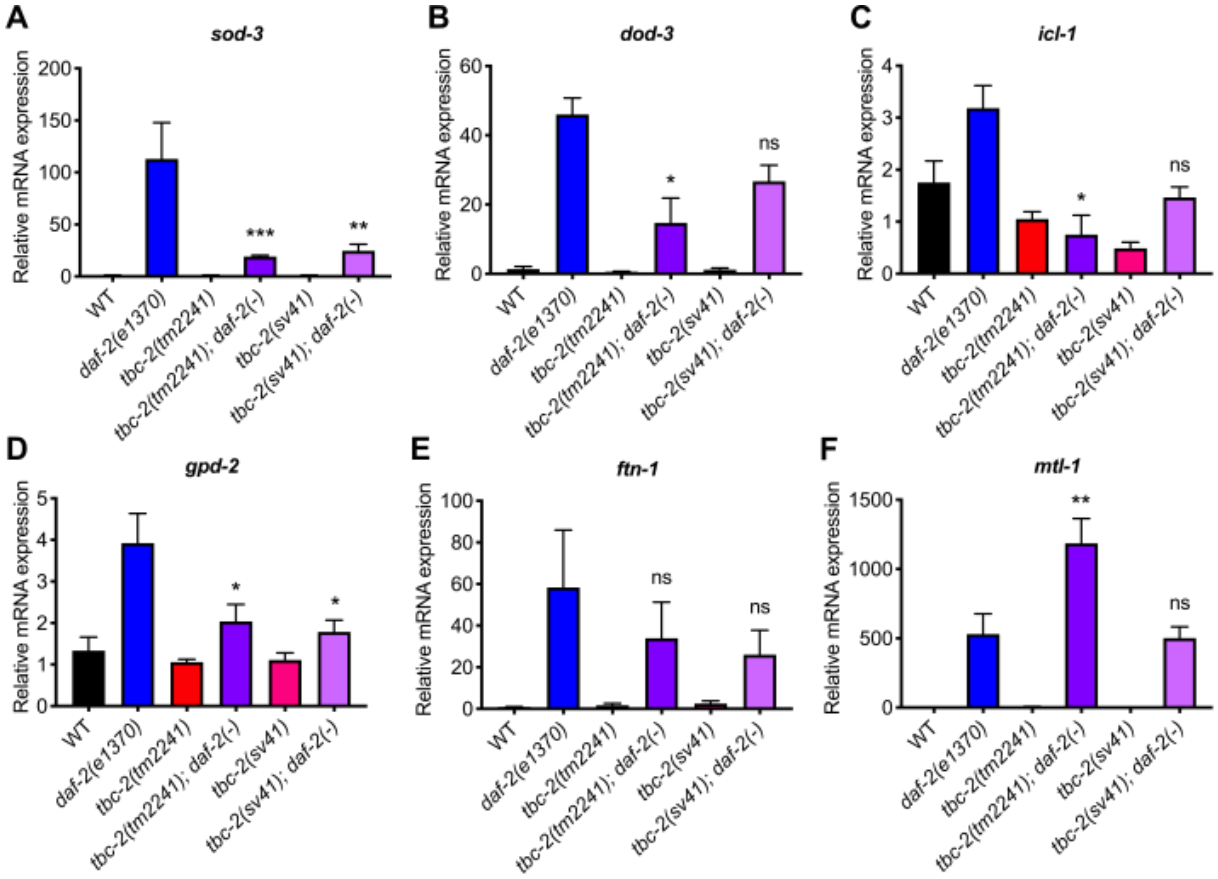

867

868 **Figure 5. TBC-2 is required for the increased DAF-16 target gene expression resulting**
869 **from decreased insulin/IGF signaling**

870 Quantitative RT-PCR analysis of DAF-16 target gene expression in wild-type, *daf-2(e1370)*, *tbc-*
871 *2(tm2241), tbc-2(tm2241); daf-2(e1370), tbc-2(sv41),* and *tbc-2(sv41); daf-2(e1370).* Statistical
872 analysis was performed using an Ordinary one-way ANOVA – Tukey's multiple comparisons

873 test. Shown are comparisons of *tbc-2(tm2241); daf-2(e1370)* and *tbc-2(sv41); daf-2(e1370)*

874 versus *daf-2(e1370)* single mutants. ns, not significant. *p<0.05, **p<0.01, ***p<0.001.

875

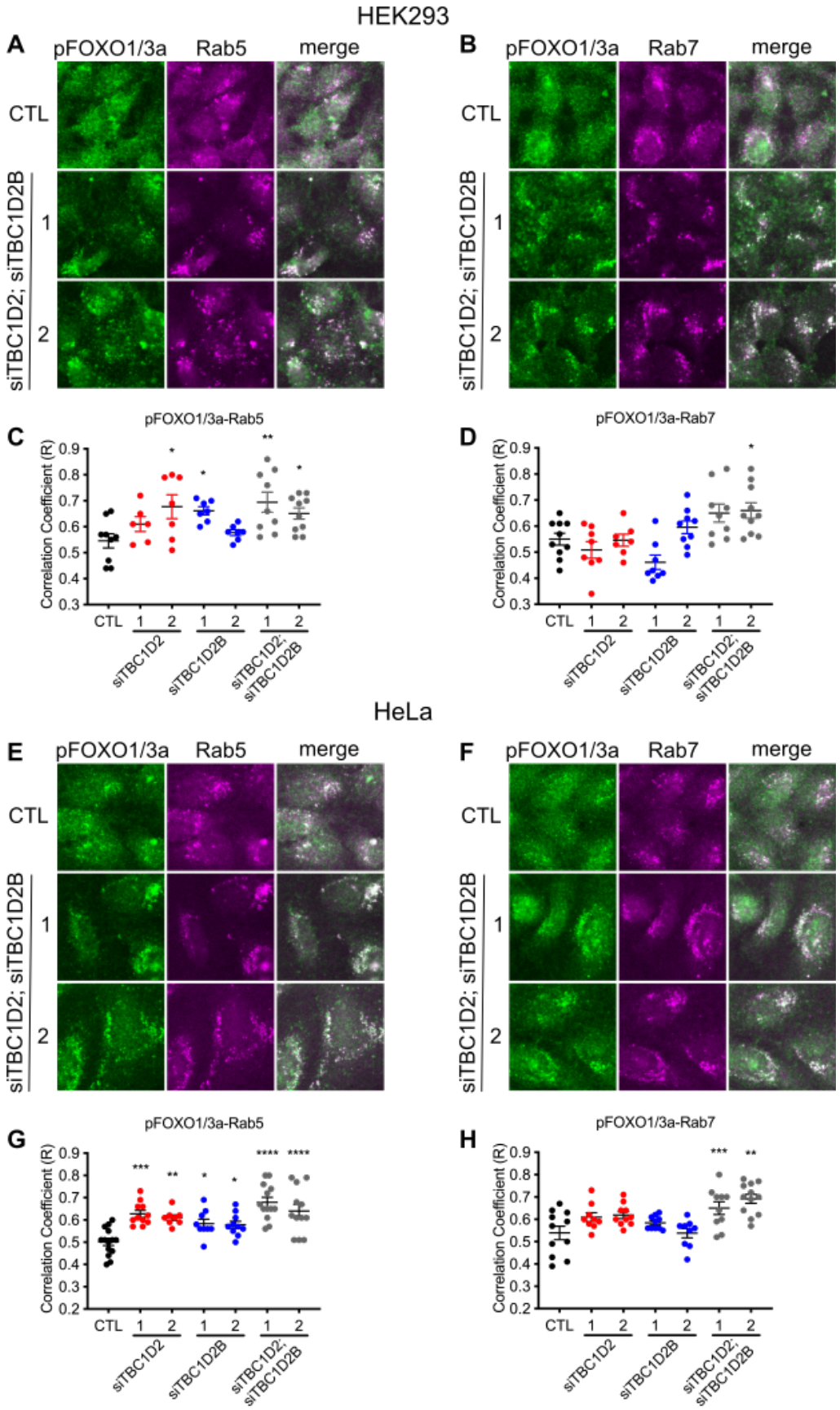

876 **Figure 6. Depletion of the human TBC-2 homologs enhances localization of phosphorylated**

877 **FOXO/DAF-16 to endosomes.** HEK293 (A-D) and HeLa (E-H) cells were transfected with
878 nonspecific control (CTL) siRNA oligonucleotides or independent oligonucleotides towards
879 TBC1D2, TBC1D2B, or both. Cells were fixed and probed for endogenous phospho-FOXO1/3a
880 (recognizes both FOXO1 and FOXO3a), Rab5 or Rab7 endosomal markers using indirect
881 immunofluorescence and visualized using a confocal microscope (63X-oil magnification with
882 4X digital zoom) 48 hours following transfection. (A,B,E,F): Representative images of indirect
883 immunofluorescence for visualization of phospho-FOXO1/3a (green), and Rab5 (A,E) or Rab7
884 (B,F) (magenta). (C,D,G,H): Coefficient of correlation between phospho-FOXO1/3a and Rab5
885 or Rab7 fluorescence intensity; a minimum of 6 images per group (n=3) with mean ± SE. * $P <$
886 0.05, ** $P < 0.01$, *** $P < 0.001$, **** $P < 0.0001$ (one-way ANOVA).
887

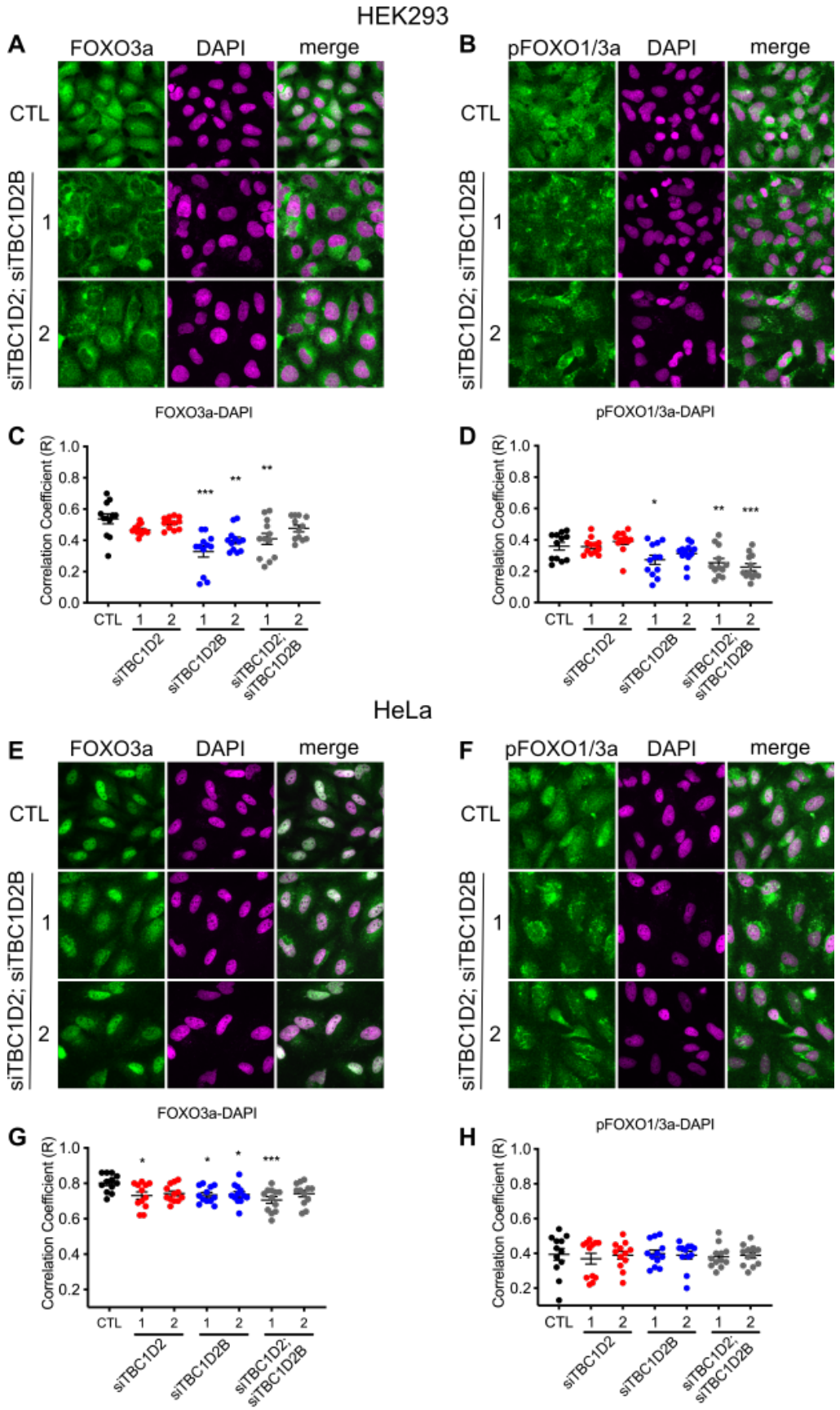

888 **Figure 7. Depletion of TBC1D2 and TBC1D2B modulates nuclear-cytosolic shuttling of**

889 **FOXO.** HEK293 (A-D) and HeLa (E-H) cells were transfected with nonspecific control (CTL)
890 siRNA oligonucleotides or independent oligonucleotides towards TBC1D2A, TBC1D2B, or
891 both. Cells were fixed and probed for pFOXO1/3a or FOXO3a using indirect
892 immunofluorescence and visualized using a confocal microscope (63X-oil magnification) 48
893 hours following transfection. (A,B,E,F): Representative images of indirect immunofluorescence
894 for visualization of endogenous pFOXO1/3a (A,E) or FOXO3a (B,F) (green) or DAPI
895 (magenta). (C,D,G,H): Coefficient of correlation between pFOXO1/3a (C,F) or FOXO3a (D,H)
896 and DAPI florescence intensity; a minimum of 6 images per group (n≥3) with mean ± SE. * $P <$
897 0.05, ** $P < 0.01$, *** $P < 0.001$ (one-way ANOVA).